Eur Radiol (2007) 17: 1879–1884
DOI 10.1007/s00330-006-0568-8

EXPERIMENTAL

J. M. Groen
M. J. W. Greuter
P. M. A. van Ooijen
M. Oudkerk

A new approach to the assessment of lumen visibility of coronary artery stent at various heart rates using 64-slice MDCT

Received: 22 May 2006
Revised: 9 November 2006
Accepted: 21 December 2006
Published online: 16 February 2007

Electronic supplementary material The online version of this article (doi:10.1007/s00330-007-0568-8) contains supplementary material, which is available to authorized users.

J. M. Groen · M. J. W. Greuter (✉) · P. M. A. van Ooijen · M. Oudkerk
Department of Radiology,
University Medical Center Groningen,
University of Groningen,
Hanzeplein 1,
P.O. Box 30001, 9700 RB
Groningen, The Netherlands
e-mail: m.j.w.greuter@rad.umcg.nl
Tel.: +31-50-3619723
Fax: +31-50-3617981
e-mail: j.m.groen@rad.umcg.nl

Abstract Coronary artery stent lumen visibility was assessed as a function of cardiac movement and temporal resolution with an automated objective method using an anthropomorphic moving heart phantom. Nine different coronary stents filled with contrast fluid and surrounded by fat were scanned using 64-slice multi-detector computed tomography (MDCT) at 50–100 beats/min with the moving heart phantom. Image quality was assessed by measuring in-stent CT attenuation and by a dedicated tool in the longitudinal and axial plane. Images were scored by CT attenuation and lumen visibility and compared with theoretical scoring to analyse the effect of multi-segment reconstruction (MSR). An average increase in CT attenuation of 144±59 HU and average diminished lumen visibility of 29±12% was observed at higher heart rates in both planes. A negative correlation between image quality and heart rate was non-significant for the majority of measurements ($P>0.06$). No improvement of image quality was observed in using MSR. In conclusion, in-stent CT attenuation increases and lumen visibility decreases at increasing heart rate. Results obtained with the automated tool show similar behaviour compared with attenuation measurements. Cardiac movement during data acquisition causes approximately twice as much blurring compared with the influence of temporal resolution on image quality.

Keywords Coronary stent · Image quality · 64-slice MDCT · Heart phantom

Introduction

The introduction of multi-detector computed tomography (MDCT) has permitted the non-invasive visualisation of coronary arteries with sufficient temporal and spatial resolution. Moreover, MDCT has been used to research the assessment of coronary artery stent patency and discrimination between the presence of in-stent stenosis. Restenosis occurs in a substantial amount of patients which have been treated with stent implantation [1]. It has been shown that no direct visualisation of coronary in-stent restenosis is feasible using four-slice MDCT due to partial volume effects and beam hardening caused by metal artifacts of the stents [2–6]. Recently it has been shown that despite some limitations 16-slice MDCT is sufficiently useful for the assessment and detection of in-stent restenosis in patients with a high accuracy in comparison with conventional coronary angiography (CAG) [7]. With the emergence of 40 and 64-slice MDCT systems the assessment of lumen visibility and diagnostic accuracy of in-stent restenosis has been improved considerably with respect to the 16-slice MDCT systems [8, 9]. The artificial lumen narrowing shows a decrease of approximately 5% and the CT attenuation is reduced by approximately 35 HU [10].

Visualisation of the in-stent lumen with 16-slice MDCT allows for the assessment of coronary artery stent patency based on the measured enhancement of contrast [11]. It has been shown that the best diagnostic quality images are obtained with a sharp edge-enhancing reconstruction

kernel, although the quality of the obtained images is hampered by increased noise levels compared with standard kernels [11–13]. The results originate from the comparison of the lumen visibility images pairs, which are reconstructed with different reconstruction kernels. The apparent lumen width is measured using a digital measuring tool included in the visualisation software. This method, however, is subjective to the observer and it is difficult to determine the exact boundary of the stents in the gradient part of the image. In addition, the image quality of the stents is very sensitive to the movement of the heart and image quality diminishes at heart rates higher than 75 beats per min (bpm) [14, 15].

In previous studies, a patient population was used to investigate image quality of coronary artery stents at high and low heart rates on four- and 16-slice MDCT [14, 15]. To our knowledge no systematic study has been published about the image quality of coronary artery stents on 64-slice MDCT. In this study, we therefore aimed at describing the correlation of image quality of coronary artery stents and heart rate using 64-slice MDCT in an ex-vivo setting by using an anthropomorphic moving heart phantom.

The purpose of our study was to assess the lumen visibility of coronary artery stents at various heart rates with an automated objective method using a moving heart phantom on a 64-MDCT system.

Theory

Coronary imaging is hampered by motion artefacts originating from the relative large velocity scale of the coronary arteries within the cardiac cycle compared with the temporal resolution of the MDCT acquisition technique [16]. This movement results in motion artefacts in the reconstructed images, expressed as blurring. The amount of blurring depends on (1) the amount of movement of the imaging target MS and (2) the acquisition time (AT). The amount of movement of the coronary artery is a function of the heart rate (HR) of the patient. The temporal resolution of a MDCT system is a function of the reconstruction method used and HR [17, 18]. This means that the resulting image quality (IS) can be expressed as

$$IS = g * MS(HR) + (1 - g) * AT(HR) \quad (1)$$

in which MS describes the amount of movement of the coronary artery as a function of heart rate, AT describes the acquisition time as a function of heart rate and g is a weight factor.

The heart rates can be ranked from low to high. With this ranking, a relative grading can be made for the function MS. In addition, the acquisition times can be ranked from high to low. With this ranking, a relative grading can be made for the function AT. The results of this grading are shown in Electronic supplementary material (ESM) Table 1, where a high score implies a high image quality. Since there is no cardiac movement at 0 bpm, this heart rate was graded with the highest score for both factors.

Materials and methods

Nine commercially available stents were used and stent dimensions were measured using a digital calliper. The stent properties are summarised in ESM Table 2.

The stents were inserted into plastic tubes and the tubes were filled with contrast fluid (Visipaque 320, Amersham Health, Little Chalfont, UK) diluted to an attenuation value of approximately 200 HU simulating contrast enhanced blood. The tubes were wrapped in horse fat with an attenuation value of −100 HU to simulate the in vivo situation of epicardial fat (Fig. 1 *left*).

Next, the stents were attached to a silicon, moving, anthropomorphic heart phantom (Limbs & Things, Bristol, UK) with artificial coronary arteries (Elastrat, Geneva, Switzerland) (Fig. 1 *right*). The phantom is connected to a respirator, which was used to control the heart rate. The heart rate was set at values of 0, 50, 60, 70, 80, 90 and 100 bpm.

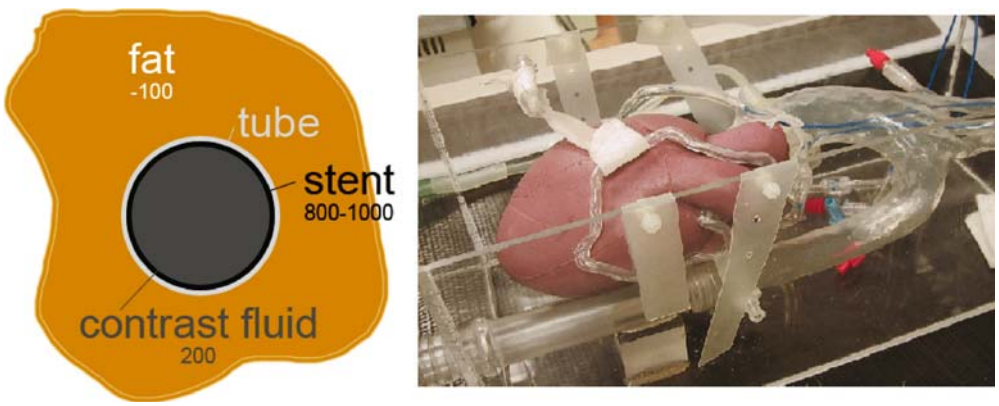

Fig. 1 *Left:* schematic figure showing the experimental setup of the contrast fluid filled tube surrounded by horse fat in the axial plane. The numbers depict the HU values of the different relevant structures. *Right:* moving anthropomorphic heart phantom with artificial coronary arteries

Measurements have been performed on a 64-detector CT-scanner (Somatom Sensation 64, Siemens, Forchheim, Germany). The scan parameters were 120 kV, 120 mAs, 370 ms rotation time and 64×0.6 mm collimation.

Image reconstruction was performed using a sharp convolution kernel (Siemens B46f) with a reconstruction slice width of 0.75 mm and a 0.5-mm increment. ECG-gating was used during scanning and the images were retrospectively reconstructed at 25% of the RR-interval corresponding to maximum expansion of the heart phantom.

Afterwards the stents were visualised on an Aquarius workstation version 3.3 (Terarecon, San Mateo, USA). We used two independent methods to asses the lumen visibility of the stents in the reconstructed images. In the first method, the average HU-value in the stent lumen was manually measured with a standard region of interest (ROI) technique. A window level/width of 300/800 was used for visualisation with an average ROI of 5.0 mm^2 and 3.9 mm^2 in the longitudinal and axial plane, respectively (Fig. 2). The lumen measurements were used to calculate the mean CT attenuation in the stent lumen. In the second automated method, screenshots were taken from every stent in the longitudinal and the axial plane with a window level/width of 512/2,048. The screenshots were used to perform the automated lumen visibility measurements using a dedicated tool.

The automated lumen visibility measurements were performed with an Automatic Stent Visibility Calculation (ASVC), a custom-build Matlab tool (The Mathworks, Natick, USA). The tool constructs the average attenuation profile through the stent in the longitudinal and axial plane. The calculation of the average attenuation profile in the longitudinal plane is done as follows; attenuation profiles are calculated from position A to B for every image line perpendicular to the stent central axis, where the position A and B are determined by the user (Fig. 3 *left*). The average longitudinal profile is calculated from the individual longitudinal profiles. The calculation of the average attenuation profile in the axial plane is doen as follows: after determination of the centre of the stent by the user, 180 attenuation profiles are calculated evenly distributed around the centre (Fig. 3 *right*). The average axial attenuation profile is calculated from the individual axial profiles.

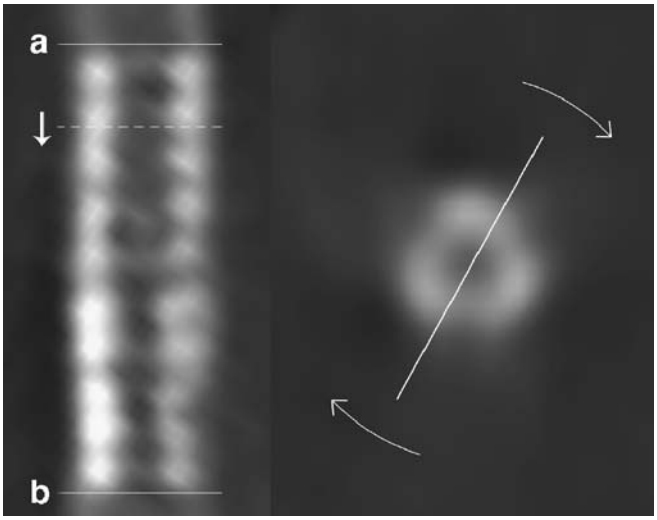

Fig. 3 Stent images (*left:* Jostent Stent Graft at 60 bpm; *right:* Taxus at 80 bpm) showing the positions of the individual profiles for calculation of the average stent profile in the longitudinal plane (*left*) and the axial plane (right)

The profile depth of the lumen (D), the full width at half maximum (FWHM) and the total width (TW) are calculated from both average profiles (ESM Fig. 4).

We define the percentual width (W_p) as a percentage of the FWHM and TW

$$W_p = (FWHM/TW) * 100\% \quad (2)$$

The percentual width is used instead of the absolute width to compensate for different magnifications of the stent images.

From the profile depth (D) and W_p, the lumen visibility (LV) is defined by

$$LV = \left(D * W_p\right)/1000 \quad (3)$$

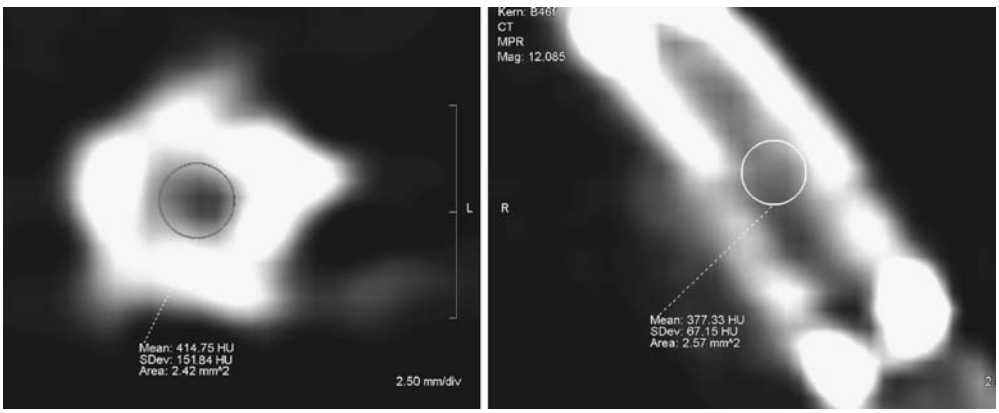

Fig. 2 Measuring the CT attenuation in the lumen. *Left:* measurements in the axial plane, Lekton Motion at 60 bpm. *Right:* measurements in the longitudinal plane, Lekton2 at 90 bpm. Calculated by the Aquarius workstation are mean HU-value, standard deviation and area of ROI

If the left and right edge of the attenuation profile are at different heights, D is calculated from the average height.

The stent images at individual heart rates were ranked according to their CT attenuation (7=least attenuation, 1=most attenuation), FWHM (7=largest width, 1=smallest width) and D (7=largest depth, 1=smallest depth) in the axial and longitudinal plane.

The difference between the CT attenuation values in the axial and longitudinal plane were compared using the Wilcoxon test at a significance level of 5%. The correlation between heart rate and CT attenuation, and the correlation between heart rate and LV, were analysed by calculating the Spearman rank correlation coefficient at the significance level of 5%.

Results

CT attenuation in the stent lumen

The results for the HU-value measurements are summarised in ESM Tables 3 and 4 for the longitudinal and axial plane, respectively. The CT attenuation in the stent lumen was calculated for each heart rate and the results are shown for the longitudinal and axial plane in ESM Figs. 5 and 6, respectively. The error margins have been omitted to improve readability of both figures.

All stents showed increased attenuation with increasing heart rate in the longitudinal plane. The CT attenuation in the longitudinal plane showed an increase from 0 to 100 bpm between 75 and 221 HU for the Taxus and Bx Sonic stent, respectively. The average increase was 139±49 HU. The average Spearman coefficient for all stents was 0.66.

All stents showed increased attenuation with increasing heart rates in the axial plane. The CT attenuation in the axial plane showed an increase from 0 to 100 bpm between 76 and 252 HU for the Bx Sonic, Multi-link Zeta and the Jostent, respectively. The average increase was 148±69 HU from 0 to 100 bpm. The average Spearman coefficient in the axial plane was 0.58. The average increase of CT attenuation over both planes was 144±59 HU.

Using the ASVC, the FWHM and depth of the stent profile were determined. The results for the FWHM are summarised in ESM Tables 5 and 6; the results for the profile depth are summarised in ESM Tables 7 and 8. The standard deviation for every measurement is given in parentheses.

The LV was calculated using equations 2 and 3 at each HR using the measured width FWHM and depth D. The data are plotted in ESM Figs. 7 and 8 for the longitudinal and axial plane, respectively, and have been fitted to a line. Error margins have been omitted to improve readability.

All stents showed decreasing LV with increasing heart rate in the longitudinal plane. The LV decreased from 0 to 100 bpm between 7.5% and 48.6% for the Taxus and Cypher stent respectively. The average decrease in LV was 26.8±13.4%. The average Spearman coefficient was 0.47.

All stents showed decreasing LV with increasing heart rates in the axial plane. The LV decreased from 0 to 100 bpm between 19.8% and 48.8% for the Lekton and Multi-link Zeta stent respectively. The average decrease in LV was 30.9±10.4%. The average Spearman coefficient was 0.58. The average decrease of LV over both planes was 29±12%.

Image scoring

The measurements are shown in ESM Fig. 9 after grading and averaging as described in the methods section. From a least squares fit, we found an optimal value of $g=0.63\pm0.06$.

Discussion

Coronary artery stenting is a successful method to treat stenosis. However, re-stenosis in the stent may happen after the procedure. This makes check-ups a necessary procedure to perform [19, 20]. MDCT is one the candidates for visualisation of the lumen of coronary artery stents. Although the results look promising, the image quality is hampered by cardiac movement and metal artefacts [21, 22]. This may result in blurred images and an exaggerated thickness of the stent struts compromising the visibility of the lumen. The 64-MDCT scanner has increased spatial and temporal resolution compared with previous CT scanner generations [23, 24] and increased LV of coronary stents is expected with these new scanners. Although 64-MDCT imaging of coronary artery stents show an improved image quality with respect to previous CT scanners, the images still show blooming artefacts and blurring [9].

The apparent width is measured in a generally accepted method to assess the stent lumen, but this method is very subjective to the user [25]. In contrast, our method, developed in this study to analyse the stent lumen, is an automated method. It enables the possibility of a systemic evaluation of the stent lumen at various heart rates. The in vivo conditions were approached as much as possible using contrast fluid and fat.

Influence of increasing heart rate

To our knowledge there have been no previous studies systematically investigating the relation between heart rate and image quality of coronary stents using 64-MDCT. There are, however, some studies with 16-slice MDCT assessing coronary arteries, which concluded that for successful cardiac imaging a heart rate below 75 or 70 bpm is necessary [14, 15, 26–29]. In a study with 40-MDCT by Gaspar et al. [8], patients were given an oral beta-blocker if their heart rate was higher than 65 bpm, and

in a study with 64-MDCT, patients were given beta-blockers if their heart rate was higher then 70 bpm [30]. Ferencik et al. [23, 30] concluded that a low heart rate is an important prerequisite for excellent image quality.

ASVC

Two different methods were used to assess the relationship between heart rate and image quality of coronary stents. The first method, the CT attenuation measurement, is a commonly used method. The second method, the ASVC technique, is a new approach. Both methods show a negative correlation between image quality and heart rate as expressed by the linear fits. The fits, however, show small significance. This small significance can be explained by the fact that the image quality does not depend entirely on heart rate, which shows a linear behaviour, but also on temporal resolution, which shows a non-linear behaviour, as can be seen from ESM Fig. 9. Despite the poor quality of the fit, the results obtained with this new ASVC method are in agreement with previous studies using generally accepted methods as stated before. Therefore, we conclude that our developed tool is a valid method for the analysis of coronary stent lumen.

Image scoring

The image scoring results (Fig. 9) show a varying resemblance between the theoretical scoring and the measured scoring. This resemblance depends on the proportion g and varies between 0 (IS completely depends on AT) and 1 (IS completely depends on MS). The best resemblance was found for g=0.63. This implies that the cardiac movement causes almost twice as much blurring in the CT image compared with blurring caused by the limited temporal resolution of the acquisition method. Multi-segment reconstruction (MSR) has been developed to further increase the temporal resolution [6, 18, 32]. The data acquisition at a rotation time of 370 ms and a HR> 65 bpm has been performed during two consecutive heart cycles using a two-segment MSR. At heart rates of 70 and 90 bpm, the data acquisition is approximately evenly distributed over two consecutive heart cycles. At 80 and 100 bpm, however, the majority of data is acquired in the first heart cycle, and the remaining portion in the second heart cycle. From Fig. 9, we can deduce that for HR of 70 and 90 bpm the measured IS is smaller than the theoretical IS. For HR of 80 and 100 bpm, the measured IS is larger than the measured IS. From this we can conclude that it is beneficial to the image quality to acquire during one cycle and that the MSR technique is not beneficial to image quality. In contrast to this, Halliburton et al. [31] showed that MSR is beneficial for 16-slice MDCT. Two other studies concluded that MSR was not beneficial to the image quality for four-slice MDCT, in accordance with our results [31, 32]. This can be explained by the fact that the coronary artery has to be in exactly the same position in the two heart cycles for the MSR algorithm to work properly. However, in general the starting position of the arteries at the beginning of the heart cycle will not exactly be the same as in the previous heart cycle. This phenomenon will introduce additional motion artefacts which result in extra blurring to the image, as has been shown before by Greuter et al. [33].

Reducing blurring

Cardiac movement and limited temporal resolution will introduce blurring in CT images of coronary arteries. The result for image scoring showed that the influence of cardiac movement is almost twice as large as the influence of the temporal resolution. To reduce blurring, it is therefore more efficient to reduce the heart rate than to increase the temporal resolution.

Limitations

These results have been obtained using a moving heart phantom. It remains uncertain how well these results are applicable to patients. However, a previous study showed that the movement of the heart phantom is a good approximation to the in-vivo situation [18]. Furthermore, in order to approach the in-vivo situation as close as possible, contrast fluid and fat were used, with CT attenuation values equal to those in-vivo.

Screenshots captured with the visualisation software were used to perform LV measurements. A loss of information is expected due to image compression used in the .jpg format of the screenshots. However, a comparison between the screenshot method and direct analysis using dicom files showed no observable difference in results.

Conclusion

We have shown that at increasing heart rates the CT attenuation in the stent increases and the lumen visibility decreases. A new approach to asses the stent lumen has been described which shows similar results to CT attenuation measurements and previous studies. The cardiac movement during data acquisition causes approximately twice as much blurring compared with the influence of temporal resolution. We conclude that a lowering of the heart rate is more beneficial to image quality than using a multi-sector reconstruction technique. In addition, we conclude that it is beneficial to image quality to acquire data in one cardiac cycle.

References

1. Gordon PC, Gibson CM, Cohen DJ, Carrozza JP, Kuntz RE, Baim DS (1993) Mechanisms of restenosis and redilation within coronary stents-quantitative angiographic assessment. J Am Coll Cardiol 21:1166–1174
2. Maintz M, Grude M, Fallenberg M et al (2003) Assessment of coronary arterial stents by multislice-CT angiography. Acta Radiol 44:597–603
3. Nieman K, Cademartiri F, Raaijmakers R et al (2003) Noninvasive angiographic evaluation of coronary stents with multi-slice spiral computed tomography. Herz 28:136–142
4. Krüger S, Mahnken A, Sinha A et al (2003) Multislice spiral computed tomography for the detection of coronary stent restenosis and patency. Int J Cardiol 89:167–172
5. Schuijf J, Bax J, Jukema W et al (2004) Feasibility of assessment of coronary stent patency using 16-slice computed tomography. Am J Cardiol 94:427–430
6. Flohr T, Küttner A, Bruder H et al (2003) Performance evaluation of a multi-slice CT system with 16-slice detector and increased Gantry rotation speed for Isotropic Submillimeter imaging of the heart. Herz 28:7–19
7. Kitagawa T, Fujii T, Tomohiro Y, Maeda K, Kobayashi M, Kunita E, Sekiguchi Y (2006) Noninvasive assessment of coronary stents in patients by 16-slice computed tomography, International Journal of Cardiology. Int J Cardiol 109:188–194
8. Gaspar T, Halon DA, Lewis BS et al (2005) Diagnosis of coronary in-Stent restenosis with multidetector row spiral computed tomography. J Am Coll Cardiol 46:1573–1579
9. Maintz D, Seifarth H, Raupach R et al (2005) 64-slice multidetector coronary CT angiography: in vitro evaluation of 68 different stents. Eur Radiol 7:1–9
10. Rist C, Nikolaou K, Flohr T, Wintersperger BJ, Reiser MF, Becker CR (2006) High-resolution ex vivo imaging of coronary artery stents using 64-slice computed tomography-initial experience. Eur Radiol 16:1564–1569
11. Hong C, Chrysant G, Woodard P et al (2004) Coronary artery stent patency assessed with in-stent contrast enhancement measured at multi-detector row CT angiography: initial experience. Radiology 233:286–291
12. Maintz D, Seifarth H, Flohr T et al (2003) Improved Coronary artery stent visualization and in-stent stenosis detection using 16-slice computed-tomography and dedicated image reconstruction technique. Invest Radiol 38:790–795
13. Seifarth H, Özgün M, Raupach R et al (2006) 64- Versus 16-slice CT angiography for coronary artery stent assessment: in vitro experience. Invest Radiol 41:22–27
14. Hong C, Becker C, Huber A et al (2001) ECG-gated reconstructed Multi-Detector row CT coronary angiography: effect of varying trigger delay on image quality. Radiology 220:712–717
15. Leber A, Knez A, Becker C et al (2003) Non-invasive intravenous coronary angiography using electron beam tomography and multislice computed tomography. Heart 89:633–639
16. Achenbach S, Ropers D, Holle J, Muschiol G, Daniel WG, Moshage W (2000) In-plane coronary arterial motion velocity: measurement with electron-beam CT. Radiology 216:457–463
17. Flohr T, Ohnesorge B (2001) Heart rate adaptive optimization of spatial and temporal resolution for electrocardiogram-gated multislice spiral CT of the heart. J Comput Assist Tomogr 25:907–923
18. Greuter MJW, Dorgelo J, Tukker WGJ, Oudkerk M (2005) Study on motion artifacts in coronary arteries with an anthropomorphic moving heart phantom on an ECG-gated multidetector computed tomography unit. Eur Radiol 15:995–1007
19. Lee CW, Park DW, Lee BK et al (2006) Predictors of restenosis after placement of drug-eluting stents in one or more coronary arteries. Am J Cardiol 97:506–511
20. Narins CR, Holmes DR Jr, Topol EJ (1998) A call for provisional stenting: the balloon is back! Circulation 97:1298–1305
21. Maintz D, Juergens K, Wichter T et al (2003) Imaging of coronary artery stents using multislice computed tomography: in vitro evaluation. Eur Radiol 13:830–835
22. Amano Y, Ishihara M, Hayashi H et al (1999) Metallic artifacts of coronary and iliac arteries stents in MR angiography and contrast-enhanced CT. Clin Imaging 23:85–89
23. Cademartiri F, Runza G, Belgrano M et al (2005) Introduction to coronary imaging with 64-slice computed tomography. Radiol Med (Torino) 110:16–41
24. Flohr T, Stierstorfer K, Raupach R et al (2004) Performance evaluation of a 64-slice CT system with z-flying focal spot. Rofo 176:1803–1810
25. Suzuki S, Furui S, Kaminaga T et al (2005) Evaluation of coronary stents in vitro with CT angiography: Effect of stent diameter, convolution kernel, and vessel orientation to the z-axis. Circ J 69:1124–1131
26. Becker CR, Schoepf UJ, Reiser MF (2001) Methods for quantification of coronary artery calcifications with electron beam and conventional CT and pushing the spiral CT envelope: new cardiac applications. Int J Cardiovasc Imaging 17:203–211
27. Hamoir X, Flohr T, Hamoir V et al (2005) Coronary arteries: assessment of image quality and optimal reconstruction window in retrospective ECG-gated multislice CT at 375-ms gantry rotation time. Eur Radiol 15:296–304
28. Nieman K, Rensing B, Geuns R-J et al (2002) Non-invasive coronary angiography with multislice spiral computed tomography: impact of the heart rate. Heart 88:470–474
29. Herzog C, Arning-Erb M, Zangos S et al (2006) Multi-detector row CT coronary angiography: influence of reconstruction technique and heart rate on image quality. Radiology 238:75–86
30. Ferencik M, Nomura CH, Maurovich-Horvat P et al (2006) Quantitative parameters of image quality in 64-slice computed tomography angiography of the coronary arteries. Eur J Radiol 57:373–379
31. Halliburton S, Stillman A, Flohr T et al (2003) Do segmented reconstruction algorithms for cardiac multi-slice computed tomography improve image quality? Herz 28:20–31
32. Juergens KU, Maintz D, Grude M et al (2005) Multi-detector row computed tomography of the heart: does a multi-segment reconstruction algorithm improve left ventricular volume measurements? Eur Radiol 15(1):111–117
33. Greuter MJW, Flohr T, Van Ooijen PMA, Oudkerk M (2006) A model for temporal resolution of multi-detector computed tomography of coronary arteries in relation to rotation time, heart rate and reconstruction algorithm. Eur Radiol, doi 10.1007/s00330-006-0228-z